Title	Exploiting implicit information from data for linear macromodeling
Author(s)	Lei, Chi-Un
Citation	IEEE Transactions on Components, Packaging and Manufacturing Technology, 2013, v. 3, n. 9, p. 1570-1577
Issued Date	2013
URL	http://hdl.handle.net/10722/198766
Rights	©2013 IEEE. Personal use of this material is permitted. However, permission to reprint/republish this material for advertising or promotional purposes or for creating new collective works for resale or redistribution to servers or lists, or to reuse any copyrighted component of this work in other works must be obtained from the IEEE.

Exploiting Implicit Information from Data for Linear Macromodeling

Chi-Un Lei

***Abstract*— In macromodeling, data points of sampled structure responses are always matched to construct linear macromodels for transient simulations of packaging structures. However, implicit information from sampled data has not been exploited comprehensively to facilitate the identification process. In this paper, we exploit implicit information from the sampled data for linear marcomodeling. First, in order to include complementary data for a more informative identification, we propose a discrete-time domain identification framework for frequency-/time-/hybrid-domain macromodeling. Second, we introduce pre-/post-processing techniques (e.g., *P*-norm identification criterion and warped frequency-/hybrid-domain identification) to interpret implicit information for configurations of identifications. Various examples from chip-level to board-level are used to demonstrate the performance of the proposed framework.**

***Index Terms*— Discrete-time domain, frequency warping, hybrid-domain, implicit information, macromodeling, *P*-norm identification, system identification, vector fitting.**

I. Introduction

With the increasing operation frequency and decreasing feature size of circuits, high-frequency signal integrity (SI) effects have become a dominant factor limiting integrated circuit (IC) system performance [1]. Accurate and efficient simulation is required during the IC design phase to capture high-frequency SI behaviors of electronic systems. Linear macromodeling, in this context, refers to replacing a high-order system by a small-order linear model with similar input–output responses, for computationally efficient simulation.

In contrast to other linear macromodeling techniques [2], [3] for broadband system identification, vector fitting (VF) [4], [5] involves iterative linear least-squares (LS) solves with a continuous-time domain (s-domain) partial fraction basis to match sampled data points. VF avoids ill-conditioned high-frequency component calculation, and therefore works in a more robust manner. However, due to the iterative pole-based calculation framework, the numerical calculation of VF is deteriorated by: 1) the dynamic behavior and the initial-guess of pole-based basis, and 2) the distribution of sampled data.

Data points unilaterally describe characteristics of the system. Meanwhile, implicit hidden information from sampled data, such as delay time, signal energy, data point distribution, signal/noise distribution, and low-/high-frequency characteristics, are potentially valuable to describe the sampled system. However, this information often has not been interpreted to facilitate the identification process. In our opinion, a proper interpretation of implicit information can lead to a realistic and accurate identification. For example, sampled data of packaging responses in s-domain are often logarithmically distributed. This distribution leads to an ill-conditioned numerical computation. Therefore, VF and a generalization of VF using discrete-time domain (z-domain) rational bases have been proposed for system identifications with an improved numerical conditioning [6]–[10]. However, existing studies have not comprehensively exploited implicit information from sampled data for identifications. Thus, input data are not maximally informative for identifications. This issue has not been explored thoughtfully by researchers, yet, is significant. It is because amount and content of data can affect properties and quality of the identification process.

In this paper, we generalize our preliminary study of z-domain macromodeling in [10] and propose techniques to interpret implicit information to facilitate the macromodeling process. In particular, we aim to develop an identification framework that matches data points of sampled responses as well as to include physical insights from the packaging field and implicit information, for a more informative (and thus, accurate) identification process. To summarize, the contributions of our work are fourfold and as follows.

1) A hybrid-domain identification framework is proposed for a more informative identification, based on complementary response information provided from time-sampled data and frequency-sampled data.
2) Frequency warping for frequency-/hybrid-domain macromodeling is proposed for a well-conditioned computation, based on the adaptive matching the way the information is recorded in the sampled data.
3) *P*-norm identification framework is proposed for a more realistic identification, based on the characteristic information of signals provided from sampled responses.
4) Pre-processing techniques (i.e., order estimation, time delay estimation, and initial pole selection) are proposed to exploit implicit information with the sampled response for identifications with suitable configuration.

In this manuscript, we introduce hybrid-z-domain macromodeling and various pre-processing techniques in Sections II and III, respectively. Examples then confirm the remarkable performance of the macromodeling framework in Section IV.

II. Macromodeling in the Hybrid-z-Domain

The I/O characteristics of the structure can be described by the I/O response data. Generally, for a

Manuscript received June 29, 2012; accepted January 20, 2013. Date of publication February 20, 2013; date of current version September 7, 2013. Recommended for publication by Associate Editor J. Tan upon evaluation of reviewers' comments.

The author is with the Department of Electrical and Electronic Engineering, The University of Hong Kong, Hong Kong (e-mail: culei@eee.hku.hk).

Color versions of one or more of the figures in this paper are available online at http://ieeexplore.ieee.org.

Digital Object Identifier 10.1109/TCPMT.2013.2245179

single-port system, macromodeling techniques intend to fit a linear time-invariant system to the desired z-domain response $H(z)$ at a set of calculated/sampled points at the I/O ports.

In z-domain macromodeling [11], [12], the s-domain system response $f(t)$ is sampled through a finite L-point, uniformly sampled ideal impulse sequence, with a sampling time T_s. The obtained z-domain data $F(z)$ is then used to construct the z-domain macromodel $\hat{F}(z)$

$$\sum_{k=0}^{L} f(k) z^{-k} = F(z) \approx \hat{F}(z) = \sum_{n=0}^{N} p_n z^{-n} \Big/ \sum_{n=0}^{N} q_n z^{-n}. \tag{1}$$

Compared to s-domain macromodeling, z-domain macromodeling usually has a computation with a better numerical condition because of the data distribution. In broadband structure macromodeling, s-domain system frequency responses are usually logarithmically sampled. Furthermore, poles of approximated systems in s-domain are un-bounded and usually logarithmically distributed. Meanwhile, z-domain system sampled responses are relatively evenly distributed, and stable poles in the z-domain are bounded within the unit circle, so the identification in the z-domain has a more numerically favorable computation for broadband macromodeling. Because of the dual domain characteristics and well-conditioned computation, z-domain models are suitable for modeling, simulation, and analysis [11].

In this section, we discuss our proposed macromodeling algorithms for frequency-z-domain (frequency-domain) (VFz), time-z-domain (time-domain) (TD-VFz), and hybrid-z-domain (hybrid-domain) (HD-VFz).

A. Frequency-Domain Macromodeling

In this section, we aim to approximate the response $F(z)$ in the z-domain with a causal and stable rational function (1) where $p_\mu, q_\upsilon \in \Re$, $q_0 = 1$. Therefore, all poles of $\hat{F}(z)$, i.e., zeros of $Q(z)$, must lie in $|z| < 1$. Compared to the existing formulation in [6] and [7], we apply an alternative z-domain partial fraction basis for a versatile macromodeling framework construction in Section II-C.

As in VF, we use a z-domain partial fraction basis to seek a rational approximation to $F(z)$. This is done by equating (approximating) the macromodel $\hat{F}(z)$ in (1) to it, namely

$$\hat{F}(z) = \left(\sum_{n=1}^{N} \frac{c_n}{1 - z^{-1}\alpha_n} \right) + d \approx F(z) \tag{2}$$

over the (discrete) frequency range of interest. Similarly, c_n and α_n are either real or in complex conjugate pairs. To ensure stability, the set of poles $\{\alpha_n\}$ in (2) must be within the unit circle (i.e., $|\alpha_n| < 1$). Analogous to VF, suppose an initial set $\{\alpha_n^{(0)}\}$, $|\alpha_n^{(0)}| < 1$, is specified, we build

$$\underbrace{\left(\sum_{n=1}^{N} \frac{c_n}{1 - z^{-1}\alpha_n^{(i)}} \right) + d}_{(\sigma F)(z)} \approx \underbrace{\left(\left(\sum_{n=1}^{N} \frac{\gamma_n}{1 - z^{-1}\alpha_n^{(i)}} \right) + 1 \right) F(z)}_{\sigma(z)} \tag{3}$$

$i = 0, 1, \ldots, N_T$. Equation (3) is linear in its unknowns c_n, d, and γ_n. Rewriting (3) for N_f frequency points $z_k = e^{j\Omega_k}$, $\Omega_k \in [-\pi, \pi)$, $k = 1, 2, \ldots, N_f$, $N_f \gg 2N + 1$, gives an over-determined linear problem. Specifically, when $z = z_k$

$$\left(\sum_{n=1}^{N} \frac{c_n}{1 - z_k^{-1}\alpha_n^{(i)}} \right) + d - \left(\sum_{n=1}^{N} \frac{\gamma_n F(z_k)}{1 - z_k^{-1}\alpha_n^{(i)}} \right) \approx F(z_k). \tag{4}$$

Repeating (4) at the N_f frequency points, an over-determined linear system matrix equation is formed

$$Ax = b. \tag{5}$$

Using the last N elements of the LS solve of x (i.e., γ_1 to γ_N), $\sigma(z)$ of (3) can be reconstructed whose zeros, $\{\alpha_n^{(i+1)}\}$, then form the new set of starting poles in the next VFz iteration. Similar to VF analysis [4], it can be easily shown that reciprocals of zeros of $\sigma(z)$, $\{\alpha_n^{(i+1)}\}$ are obtained as the eigenvalues of

$$\Psi = \left(\begin{bmatrix} 1/\alpha_1^{(i)} & & \\ & \ddots & \\ & & 1/\alpha_N^{(i)} \end{bmatrix} + \begin{bmatrix} 1/\alpha_1^{(i)} \\ \vdots \\ 1/\alpha_N^{(i)} \end{bmatrix} \begin{bmatrix} \gamma_1 \cdots \gamma_N \end{bmatrix} \right)^{-1}. \tag{6}$$

Once a converged set of poles $\{\alpha_n^{(N_T)}\}$ are obtained at N_T iterations, the final step is to reconstruct the macromodel $\hat{F}(z)$. With reference to (3) and (4), we should now have $\sigma(z) \approx 1$ and the following relationship holds:

$$\hat{F}(z_k) = \left(\sum_{n=1}^{N} \frac{c_n}{1 - z_k^{-1}\alpha_n^{(N_T)}} \right) + d \approx F(z_k) \tag{7}$$

$k = 1, 2, \ldots, N_f$. The residues c_n of $\hat{F}(z)$ are computed in exactly the same manner as before, except that the last N elements in both A_k and x are now truncated. This partial fraction decomposition of $\hat{F}(z)$ then readily adds up to a rational function.

The response $F(z)$ in (2) may contain complex conjugate poles and residues whose time-domain transforms are also complex conjugates, thus conforming to a real response. Discussion of pole relocation of complex poles can be found in [10] and [8], and is not elaborated here.

B. Time-Domain Macromodeling

Frequency-domain macromodeling algorithms are often used to generate reduced macromodels. However, frequency-domain macromodeling requires spectral information, which involves complicated measurement/simulation. Due to its high computational cost, the full-wave analysis is usually terminated before all transient responses vanish so that truncated time responses are obtained. Macromodeling from truncated time-sampled data is therefore desirable. Different numerical techniques (e.g., [13]) have been used for identification of linear structures with time-sampled data. However, these methods are based on large-scale matrix operations and expensive singular value decompositions. Therefore, a time-domain counterpart of VF has been developed for macromodeling of

time-sampled data with lower computational cost [14], but its performance is limited by the discretization in each iteration. We, therefore, propose TD-VFz.

We start by transforming VFz to TD-VFz. As in VFz, TD-VFz uses z-domain partial fractions to seek $\hat{F}(z)$ to a *real* time-domain $F(z)$. From (3), we apply an input $W(z)$ to $F(z)$ and let $Y(z) = F(z)W(z)$ be the output. The time-domain relationship is then given by the inverse z-transform

$$y[k] \approx d\,w[k] + \sum_{n=1}^{N} c_n w_n[k] - \sum_{n=1}^{N} \gamma_n y_n[k]$$
$$y_n[k] = \left((\alpha_n^{(i)})^k u[k]\right) * y[k]\ ,\ w_n[k] = \left((\alpha_n^{(i)})^k u[k]\right) * w[k] \tag{8}$$

where $*$ denotes the convolution and $u[k]$ is the Heaviside unit-step sequence. Suppose N_t samples of the input and output sequences, $w[k]$ and $y[k]$, are captured, an over-determined linear equation is set up, as shown in [10]. Using γ_1 to γ_N, the new set of poles in the next iteration can be found through obtaining eigenvalues of (6). When a converged set of poles $\{\alpha_n^{(N_T)}\}$ are obtained, the final step is to compute residues and reconstruct the rational function $\hat{F}(z)$. The detailed computation is shown in [10] and is not further discussed here.

C. Hybrid-Domain Macromodeling Using Frequency-Sampled and Time-Sampled Response Data

We have proposed z-domain frequency-domain and time-domain macromodeling, respectively, in Section II-A and II-B. However, there are practical measurement limitations in both domains [15]. For example, time-domain measurement requires a long measurement time to capture low-frequency characteristics. Meanwhile, frequency-domain measurement requires a great deal of effort and time to obtain hundreds of GHz frequency response data. Therefore, it is practically efficient to model the structure using short time-domain measurement and tens of low-frequency frequency response data. Furthermore, information from dual domain responses can be different if frequency responses and/or time responses are under-sampled, or sampled with measurement errors. From the analysis perspective, signal integrity analyses are usually performed in the frequency domain, while global interconnect architecture simulations and eye diagram analyses are performed in the time domain. Thus, the single-domain macromodeling is not as favorable as hybrid-domain macromodeling since a completely frequency-domain approximation approach may overlook certain time-domain requirements and vice versa. These necessities have spawned the interest to develop HD-VFz for linear macromodeling.

Specifically, HD-VFz can fit both time- and frequency-sampled responses simultaneously in the LS sense via the over-determined equation (provided $N_f + N_t > 2N + 1$)

$$Ax = b \quad \text{where} \quad A = \begin{bmatrix} A_f \\ A_t \end{bmatrix} \text{ and } b = \begin{bmatrix} b_f \\ b_t \end{bmatrix} \tag{9}$$

where A_f/b_f and A_t/b_t represent A/B in VFz computation and TD-VFz computation, respectively. Using the last N elements of the LS solution of x, i.e., γ_1 to γ_N, $\sigma(z)$ of (3) can be constructed whose zeros, denoted by $\{\alpha_n^{(i+1)}\}$, then form the new set of poles in the next HD-VFz iteration, as in VFz. The zeros of $\sigma(z)$ are constructed in a similar manner to the VFz formulation in (6).

D. Building the Macromodel

The z-domain macromodel obtained from the framework can be used directly for frequency-domain analyses or fixed time step transient simulations. It can also be transformed into an equivalent circuit [11] or an s-domain system by stability- and passivity-preserving bilinear transformation. Besides constructing a rational function model, the model parameters $\{\alpha_n\}$ and $\{c_n\}$ in (2) and (8) can be used for recursive convolution for transients simulations [11].

E. Remarks for the Framework

1) Convergence Analysis of TD-VFz: TD-VFz can be regarded as a reformulation of the rational function fitting procedure called Steiglitz–McBride (SM) iteration [16]. First, given $F(z)$, SM iteration replaces the nonlinear LS approximation objective $\widehat{G}_{L_2} = \Sigma_{k=1}^{N_t} |F(z_k) - \frac{P(z_k)}{Q(z_k)}|^2$ with a linearized $\widehat{G}_{\mathrm{SM}}$ where

$$\widehat{G}_{\mathrm{SM}} = \sum_{k=1}^{N_t} \frac{1}{\left|Q^{(i-1)}(z_k)\right|^2} \left|Q^{(i)}(z_k)F(z_k) - P^{(i)}(z_k)\right|^2. \tag{10}$$

Here, $P^{(i)}$ and $Q^{(i)}$ are, respectively, the numerator and denominator determined during the ith SM iteration. Although $\widehat{G}_{\mathrm{SM}}$ is not equivalent to $\widehat{G}_{L_2}$, by using the triangle inequality, if we approximate $F(z)$ by an Nth-order system, we get $||\widehat{G}_{L_2} - \widehat{G}_{\mathrm{SM}}||_2 \le 2\sigma_{N+1}$. Here, σ_i, which denotes the ith Hankel singular value (HSV) of a Hankel-form matrix constructed by the time-domain impulse coefficients f_k's of $F(z)$ in (1), measures the significance of the Nth approximant order [17]. In general, SM iteration converges to a near-global-optimal approximant in the LS sense for noise-free data, with an *a priori* error bound for an Nth-order approximant

$$\min_{\deg(\frac{P}{Q}=N)} \left(\frac{1}{2\pi}\int_{-\pi}^{\pi} \left|F(e^{j\omega}) - \frac{P^{(i)}(e^{j\omega})}{Q^{(i)}(e^{j\omega})}\right|^2 d\omega\right)^{1/2} \le \sigma_{N+1}. \tag{11}$$

2) Selection of Initial Poles in the Framework: Initial poles assignment is required for most iterative identification frameworks. In the framework, we assign $\left\{\alpha_n^{(0)}\right\} = \{\gamma\}\, e^{j\{\theta\}}$, where $\{\gamma\}$ and $\{\theta\}$ are the sets of radii and angles of the initial poles, respectively. In framework, initial poles are uniformly distributed along the passband. For example, if there is one single passband in the interval $\left[\omega_{p_1}, \omega_{p_2}\right]$ and N is even, the initial estimates of the pole angles are $\theta_k = \omega_{p_1} + (2k-1)\,\frac{\omega_{p_2} - \omega_{p_1}}{N}$ for $k = 1, 2, \ldots, N/2$. For lowpass responses, we assign ω_{p_1} to be zero and ω_{p_2} to be the 3-dB cutoff frequency. Furthermore, responses usually have fast-changing transients, and the poles usually lie near the boundary of the unit circle. Therefore, we usually set $\{\gamma\}$ to be 0.9.

3) Selection of Iterations: The number of iterations affects the computation complexity of iterative frameworks. The step size of parameter alteration can be used as the stopping criterion, i.e., the algorithm can stop the iteration when

$$\left|\frac{\Delta p_{i,i-1}-\Delta p_{i-1,i-2}}{\Delta p_{i-1,i-2}}\right|\leq\varepsilon \tag{12}$$

where $\Delta p_{i,j}$ is the parameter difference between i-th iteration and j-th iteration and ε is a pre-defined threshold. If (12) is not satisfied within a number of iterations, we need to adjust the macromodel order for a better identification.

However, computational difficulties are also related to the characteristics of the underlying structure and sampling distributions. In situations with irregular disturbances, the approximation accuracy does not get much improved with higher order models or more iteration, which implies generalized models (e.g., grey-box models) are required for system descriptions.

4) Passivity Enforcement in the z-Domain: Similar to the case in VF, macromodels generated from the framework are not guaranteed to be passive. s-domain passivity checking/enforcement techniques [18] can be used to rectify the model, since the bilinear continue-to/from-discrete transformation is passivity-preserved [19]. Furthermore, passivity issues in z-domain systems are similar to the one in s-domain systems [19]. For example, positive real lemma [20], bounded real lemma [21] in z-domain can be used for passivity enforcement. Symplectic matrix [21] perturbation can also be developed for z-domain passivity enforcement, from the similar derivation of Hamiltonian matrix perturbation in s-domain.

III. Enhancements of Linear Macromodeling via Pre-Processing Techniques

In this section, data pre-processing techniques are introduced such that implicit information from the data is used to generate a correct macromodel.

A. Selection of Macromodel Order Based on Time-Sampled Data

Error bound (11) in TD-VFz is important as it provides a certificate for the approximation accuracy and can be used to select the approximant order for TD-VFz and HD-VFz. It is shown that the singular value of an upper triangular Hankel matrix H is equivalent to the HSVs of the impulse response system [22]. Exactly analogous to balanced truncation [22], the macromodel order N is chosen such that $\sigma_N \gg \sigma_{N+1}$. This approach gives a quantitative metric to efficiently determine the value of an appropriate macromodel order.

An efficient HSV-based computation could help users to obtain a good estimation of order in practical applications. Therefore, a partial SVD is compared with a full SVD. The result shows that the partial SVD requires excessive matrix operation to determine the first 40 singular values. However, in practice, we need to compute the first 50 singular values (the order of a general macromodel). Therefore, full SVD is a better choice in this application.

B. Macromodeling Using a P-Norm Approximation Criterion

2-norm (L_2) identification is usually used in identification frameworks [8]. However, to give a more exact and realistic description of the sampled system, the identification framework can be generalized to a P-norm (L_p) identification

$$\min\left\|\frac{N^{(t)}(z)}{D^{(t-1)}(z)}-\frac{D^{(t)}(z)}{D^{(t-1)}(z)}H(z)\right\|_p. \tag{13}$$

The identification norm can be specialized to meet different macromodeling requirements [23]. In other words, P-norm criterion is a better criterion for identifying models with a generalized p-Gaussian noise [24], i.e., L_∞ (Chebyshev norm) approximation, L_2 approximation, and L_1 approximation are more effective for identifying responses when the noise follows the Lapalace distribution, the Gaussian distribution, and the uniform distribution, respectively. The exponent P can be determined if the noise distribution is known, or estimated from the given response samples [23]. Generally, Gaussian distribution is usually used to model noise, measurement discrepancy, and packaging surface roughness [25]. However, stochastic process in the packaging simulation can also be described by the spatial (or temporal) correlation function, which can also be an exponential or other distribution.

In general, the L_∞ (Chebyshev norm) approximation, L_2 approximation, and L_1 approximation give a more accurate macromodel for linear-phase (time-delayed) responses, white-noise-contaminated responses, and impulsive-noise-contaminated responses, respectively. For example, an L_1 approximation can be used if there are analog-to-digital conversion errors and transmission bit errors in the measurement process.

C. Macromodeling of Time-Delayed Systems in z-Domain

VFz has difficulties in identifying time-delayed systems, since the cost function may be trapped at a local minimum. For time-sampled response of a single excitation pulse, the time difference between excitation pulse and resultant pulse is a natural selection of the delay. For time-sampled responses with overlapping pulses and random excitations, the delay can be identified by a cross-correlation between I/O signals

$$\tau=\max_{\tau}\left|\frac{1}{N-\tau}\sum_{t=\tau}^{N-1}y(t)\,w(t-\tau)\right|. \tag{14}$$

For frequency-sampled responses with an apparent passband, the delay can be obtained by the mean slope of the unwrapped phase of the response

$$\tau=-\frac{1}{k_2-k_1}\sum_{k=k_1}^{k_2-1}\frac{\angle F(z_{k+1})-\angle F(z_k)}{\omega_{k+1}-\omega_k} \tag{15}$$

where $[\omega_{k_1},\omega_{k_2}]$ defines the passband of the system. The delay can be included as $z^{-(T_d/T_s)}\widehat{F}(z)$ after the delay-extracted identification, where T_d is the delay time that we estimated. The proposed approach can be generalized to identify multiple delays. For example, the causality information and phase can be recovered by a z-domain Hilbert transform [26]. Meanwhile, z-domain delay can be included through inserting time shifting operators [26].

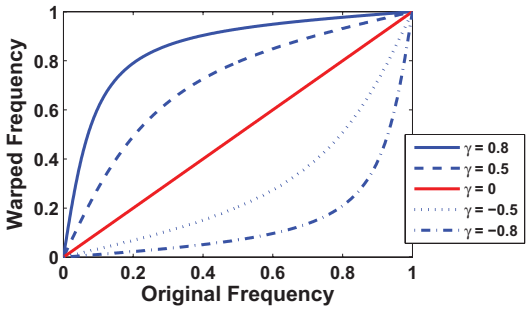

Fig. 1. Relationship of the sampled location between the z-domain (original frequency) and the $\tilde{z}$-domain (warped frequency) with different warping parameters (γ).

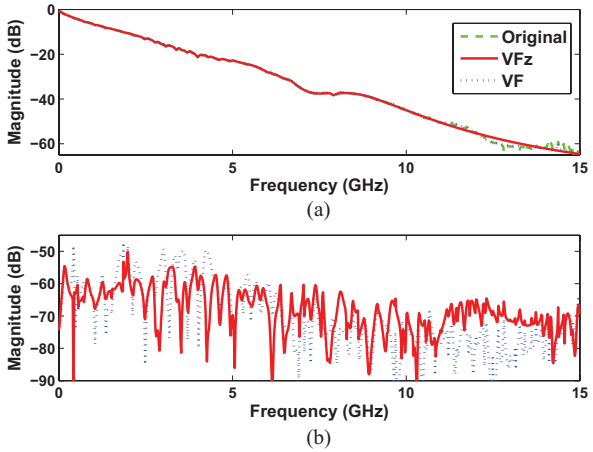

Fig. 2. Frequency responses of the channel example using VFz and VF (a) magnitude responses and (b) error in magnitude responses.

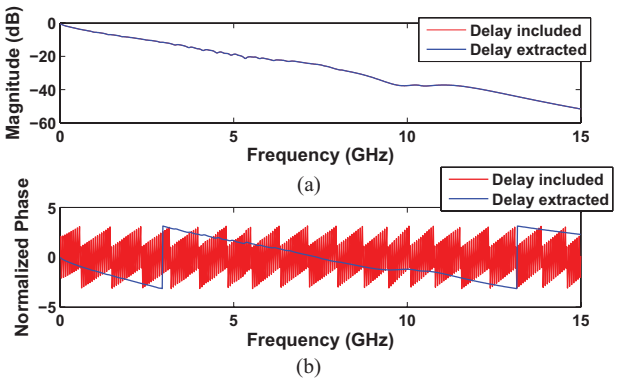

Fig. 3. Magnitude responses of the channel example using VFz (a) magnitude response and (b) phase response.

D. Frequency Warping in Frequency-/Hybrid-Domain Macromodeling

Recently, the calculation in a parameter-controlled frequency-warped z-domain ($\tilde{z}$-domain) has been introduced to improve the numerical condition in the time-domain macromodeling [27]. To further alleviate ill-conditioned computation problems in the linear macromodeling process, we have generalized the time-domain frequency warping to frequency-/hybrid-domain pre-processing process.

From the time-domain signal perspective, frequency warping can be adaptively adjusted, in order to re-interpret the recorded information in the source signal and manifest some characteristics of the signal source. In other words, frequency warping acts as a nonstationary re-sampling in time of the input signal performed by sampling the output signal of an allpass filter chain. The warping starts by replacing all operators (z^{-1}) in the original signal $G\left(z^{-1}\right)$ by allpass operators ($\tilde{z}^{-1}$) in the warped signal $H\left(\tilde{z}^{-1}\right)$ with a warping parameter γ

$$G\left(z^{-1}\right) \approx H\left(\tilde{z}^{-1}\right), \tilde{z}^{-1} = \frac{z^{-1}+\gamma}{\gamma z^{-1}+1} \tag{16}$$

then continues the macromodeling process in $\tilde{z}$ domain, finally warps the macromodel back to z^{-1} (original) domain through an inverse bilinear transform of (16).

From the frequency-domain signal perspective, frequency warping is to reshape the frequency axis. In other words, frequency warping transforms the structure response by assigning a weighting in the frequency domain and gives a higher resolution (accuracy) in the desired region. Warping of frequency-sampled response can be done through changing the location of the sampled frequency by (16) directly. The mapping of the sampled location between z-domain and $\tilde{z}$-domain of some γ values is shown in Fig. 1. From the figure, the reshaping of axis in frequency warping is linear, nonsingular, and isometric. Furthermore, we observe that the frequency warping is a mapping of a composition of a semi-sigmoid function and its inverse scaled with γ.

Frequency warping is initially proposed to identify fixed-time step responses in time-domain macromodeling, since z-domain systems have a fixed-time step property. However, this technique can also be applied in frequency-sampled responses and fixed-step hybrid-sampled responses, since they also have a fixed-time step property in z-domain. Furthermore, warping usually suffers from significant approximation errors at a high-pass response relative to half the sampling rate due to the mapping process. However, this situation is not common in SI applications. Furthermore, frequency warping can be applied to different situations, such as hybrid-domain macromodeling and multiport macromodeling, by applying a unified γ to all responses in the modeled system.

IV. Numerical Examples

In this section, we use different examples to show the performance of algorithms in modeling linear structures. The proposed algorithms are coded in MATLAB m-script (text) files and run in the MATLAB 7.4 on a 1-GB-RAM 3.4-GHz PC.

A. Macromodeling of a Differential Transmission Channel Using VFz With Performance Analysis

The test example arises from modeling a 40.5" differential transmission channel on a full mesh ATCA backplane (DTC) [28]. The single-ended four-port scattering parameters are measured at 750 frequency samples ranging from 50 MHz to 15 GHz. The four-port scattering parameters are converted to differential two-port scattering parameters. The frequency sampled response is delay-extracted and fitted using VFz and VF with a 60-pole approximant.

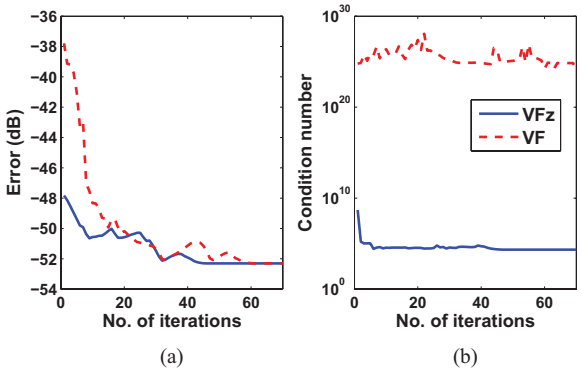

Fig. 4. Computation details of VFz with a different number of iterations. (a) Relative error. (b) Condition number of the system equation matrix.

Matrix normalization is applied to both VFz and VF to improve the numerical condition. It takes 1.90 s and eight iterations for VFz to achieve a relative error ($\|$Fitted response–Original response$\|_2/\|$Original response$\|_2$) of −50.75 dB. The average relative error of VF and VFz is 0.0024 and 0.0024, respectively. The CPU time of VF and VFz is 14.49 and 10.93 sec., respectively. Figs. 2 and 3 plot the fitted responses and show the excellent accuracy of VFz. The relative error and the condition number of the system equation matrix [A in (5)] in each iteration are shown in Fig. 4. VFz converges after 45 iterations, while VF requires 61 iterations to achieve a −52.3-dB accuracy. Compared with VF, VFz has a more numerically favorable computation, hence VFz achieves an accurate fitting in the first iteration (achieving a −48-dB error) and converges much faster. It also shows that VFz can identify board-level responses and responses with delay(s). The data set is obtained from MATLAB RF toolbox V2.4 (default.s4p).

Next, we study the fitting robustness of VFz when the data is noisy. We repeat the example but with the frequency-sampled response corrupted by white noise resulting in a signal-to-noise ratio (SNR) of 35 dB. In this case, VFz converges at a relative error of −35.34 dB.

B. Macromodeling a Power Distribution Network Using VFz

A 14 × 14 admittance parameter matrix of a system-in-package intelligent network communicator (INC) board is obtained [3], whose 1286-points response ranges from 10 KHz to 9 GHz. The tested INC board contains digital, ratio frequency (RF), and optoelectronic sections on a single 83 mm × 65 mm single test bed. By removing unnecessary computations of un-coupled responses, the identification is significantly reduced from fitting 196 responses to fitting 54 responses. The average relative error of VF and VFz is 0.0177 and 0.0189, respectively. The CPU time of VF and VFz is 682 and 271 sec., respectively. This large-scale package-level example has a large amount of response data to be fitted, but VFz is computationally well-conditioned and obtains an accurate approximation within five iterations. The data set is obtained from http://www.ece.gatech.edu/research/labs/hppdl/Epsilon2008/bemp/examples_thesis/powerplane/multiport/TMM_PRC.s14p.

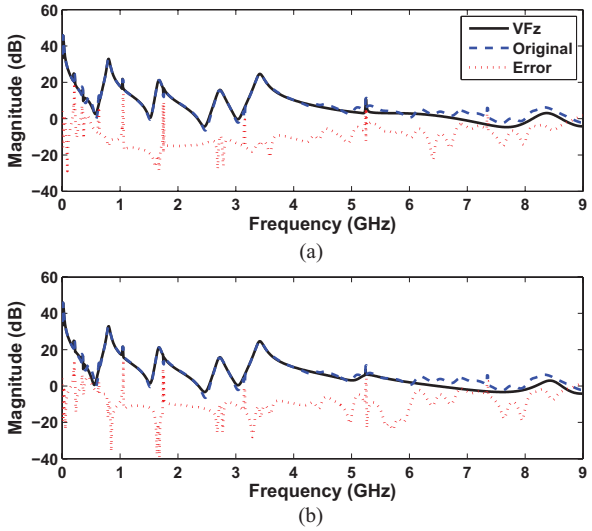

Fig. 5. Magnitude responses of the power distribution network. (a) Approximation using L_1 norm. (b) Approximation using L_2 norm.

C. Modeling a Power Distribution Network Using a P-Norm Approximation Criterion in VFz

The example arises from a power distribution network of an IC power plane ([29], page 111), whose 1286-point admittance response ranges from DC to 9 GHz. In addition, additive signals and subtractive disturbances have been included to model impulsive noise/errors from the measurement. The noise-contaminated response is fitted using VFz with a 35th-order macromodel with L_2 norm approximation and a set of linear-spaced initial poles, which gives 0.1078 L_1 and 0.0606 L_2 error in the fitting. The responses are also fitted using the L_1 norm approximation with the same configuration, which gives an approximation with 0.0996 L_1 error and 0.0546 L_2 error. The magnitude response of the converged approximation is shown in Fig. 5. It shows that in identifying responses with impulsive noise, L_1 norm approximation renders a more accurate approximation in terms of both L_1 norm and L_2 norm. Subsequently, P-norm approximation can be used as an alternative approximation criterion for approximations. The data set is obtained from http://www.ece.gatech.edu/research/labs/hppdl/Epsilon2008/bemp/examples_thesis/powerplane/oneport/Powerplane.s1p.

D. Modeling Transmission Channel Using TD-VFz

The test example arises from modeling the transmission channel in Section IV-A. The time-domain response is excited from a pre-determined 200-pole model and an ideal impulse signal ($w[0] = 1$ and $w[n] = 0$ for $n = 1, 2, \ldots, L-1$), and the sampling rate is 33.3 ps. The 500-point output signal is fitted using TD-VFz with a 25-pole approximant, ending up at a relative error of −35 dB. It takes 0.46 s (three iterations) for TD-VFz to reach convergence, while TD-VF [14] requires ∼1 s (four iterations) to achieve −27.04-dB accuracy. Fig. 6 plots the fitted responses. We observed that a poor fitting is obtained for frequency ranges with small magnitudes. Weighting functions (e.g., inverse magnitude weighting [30]) or a P-norm identification criterion can be applied for a better fitting.

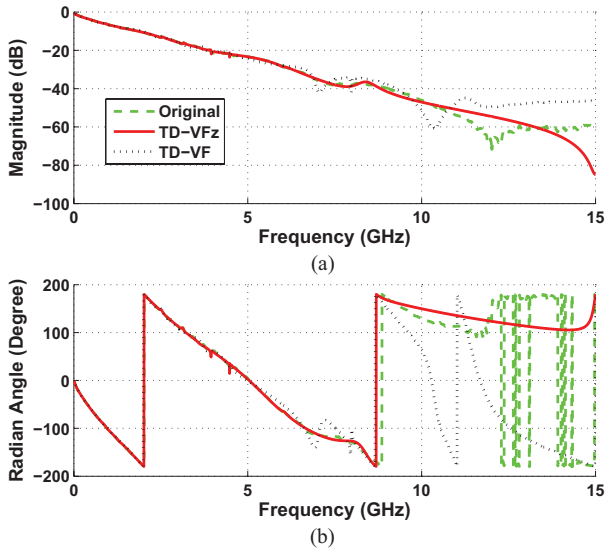

Fig. 6. Frequency responses of the channel example using TD-VFz and TD-VF. (a) Magnitude responses. (b) Phase responses.

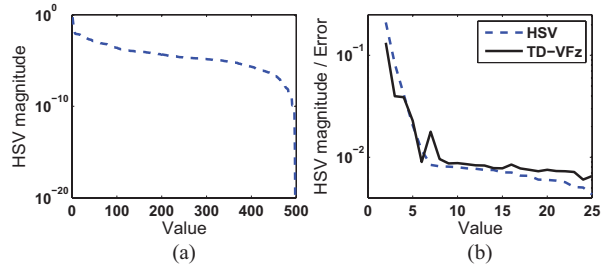

Fig. 7. HSVs of the system in the channel example. (a) All HSVs. (b) HSVs in comparison with the identification error.

We also study the robustness of TD-VFz. First, we repeat the example but with the output sequence $y[k]$ perturbed by white noise under an SNR of 35 dB. In this case, TD-VFz converges, ending up with a relative error of -31 dB.

Moreover, we investigate the use of the HSV in guiding the model order selection for TD-VFz. Fig. 7 shows the HSVs found by the impulse response channel and the relative error of different approximant orders. With excluding the numerical deviation, an evidential correlation can be seen between these two parameters. Such HSV design guideline, as far as we are aware, is unavailable in other algorithms.

E. Modeling Transmission Channel Using HD-VFz

The test example arises from modeling the transmission channel in Section IV-A. The time-sampled response signal is excited by an ideal impulse signal, and the sampling rate is 33.3 ps. Time-sampled and frequency-sampled response signals are fitted using VFz, TD-VFz, and HD-VFz with a 25-pole approximant. It takes 0.75 s (three iterations) for convergence. The quantitative comparison is shown in Table I. The identified result is shown in Fig. 8. The more time-consuming computation in HD-VFz than VFz and TD-VFz is justified by the more accurate approximation and better preservation of dual-domain characteristics, in contrast to VFz and TD-VFz, which operate completely in a single domain. This demonstrates the superiority of a dual-domain fitting property in HD-VFz.

TABLE I
RESULT OF CHANNEL MACROMODELING USING TD-VFZ, VFZ, AND HD-VFZ

	TD-VFz	VFz	HD-VFz
Number of time-sampled points	300	0	300
Number of frequency-sampled points	0	100	100
L_2 error in frequency responses	0.1366	0.1447	0.1317
L_∞ error in frequency responses	0.0258	0.0193	0.0146
L_2 error in time-domain responses	0.0036	0.0037	0.0034
L_∞ error in time-domain responses	0.0007	0.0009	0.0009
CPU time (s)	0.3594	0.2656	0.7500

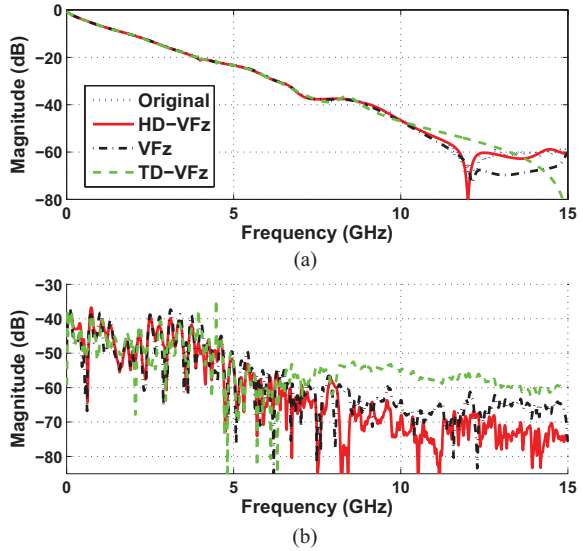

Fig. 8. Frequency responses of the channel example using VFz, TD-VFz, and HD-VFz. (a) Magnitude responses. (b) Error in the magnitude responses.

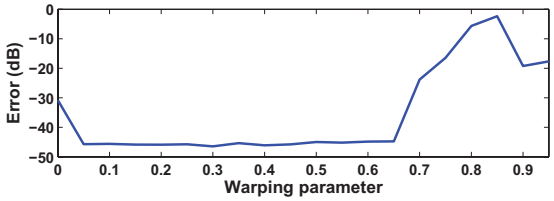

Fig. 9. L_2 error in the macromodeling examples using frequency warping with respect to warping parameters.

F. Macromodeling of a Backplane Channel With Frequency Warping Pre-Processing in VFz and HD-VFz

The scattering parameters of a 16-port high-speed backplane differential channel are simulated at 500 frequencies ranging from 0.05 to 15 GHz [28]. The frequency response of the backplane is warped using (16) with 20 uniformly distributed γ, where $0 \leq \gamma \leq 0.95$. Each warped response is approximated by a 40th-order macromodel using VFz in the $\tilde{z}$-domain. The macromodel is then mapped back to the z-domain. The result with different warping parameters is shown in Fig. 9. Results show that warping with $\gamma = 0.30$ gives the best approximation, which reduces L_2 error from 0.0287 to 0.0047, when compared to the original case ($\gamma = 0$).

Furthermore, the crosstalk between two differential channels is also modeled to generate a 60th-order macromodel with the same configuration. The L_2 error using VFz is reduced from 0.9166 to 0.0020 after applying frequency warping.

Moreover, the two responses are combined for a multiport macromodeling process. The example is then fitted using VFz with a 40th-order model. The frequency warping generates a macromodel with a minimum L_2 error 0.0104 and 0.0076 for the two responses, respectively, using $\gamma = 0.30$. The result shows that the numerical computation of identifications can be significantly improved using frequency warping. The data set is obtained from MATLAB RF Toolbox V2.4 (default.s16p).

Another test example arises from modeling the transmission channel in Section IV-A and IV-E is used for a hybrid-domain frequency warping demonstration. The L_2 error is reduced from 0.1317 to 0.1093 after applying frequency warping ($\gamma = 0.66$). Results show that there is a less error reduction in hybrid-domain warping, compared to the single-domain warping. This is because hybrid-domain data usually contain more element discrepancies in the system matrix, and thus, constitute a well-conditioned computation already.

V. Conclusion

A z-domain linear macromodeling framework was presented with exploitation of implicit information from sampled data for macromodeling. The proposed hybrid-domain identification framework, P-norm identification criterion, time-/hybrid-domain model order selection, and frequency-/hybrid-domain frequency warping interpret implicit information to facilitate the macromodeling process. Various examples confirmed that the framework exhibits an efficient computation and produces accurate macromodels for simulation.

References

[1] S. Caniggia and F. Maradei, *Signal Integrity and Radiated Emission of High-Speed Digital Systems*. New York, USA: Wiley, 2008.

[2] R. Gao, Y. S. Mekonnen, W. T. Beyene, and J. E. Schutt-Aine, "Black-box modeling of passive systems by rational function approximation," *IEEE Trans. Adv. Packag.*, vol. 28, no. 2, pp. 209–215, May 2005.

[3] S. H. Min, "Automated construction of macromodels from frequency data for simulation of distributed interconnect networks," Ph.D. dissertation, Georgia Inst. Technol., Public Res. Univ., Atlanta, GA, USA, 2004.

[4] B. Gustavsen and A. Semlyen, "Rational approximation of frequency domain responses by vector fitting," *IEEE Trans. Power Del.*, vol. 14, no. 3, pp. 1052–1061, Jul. 1999.

[5] C. U. Lei, Y. Wang, Q. Chen, and N. Wong, "A decade of vector fitting development: Applications on signal/power integrity," *IAENG Trans. Eng. Technol.*, vol. 5, pp. 435–449, Oct. 2010.

[6] Y. S. Mekonnen and J. E. Schutt-Aine, "Broadband macromodeling of sampled frequency data using z-domain vector-fitting method," in *Proc. IEEE Workshop Signal Propag. Interconnects*, May 2007, pp. 45–48.

[7] B. Nouri, R. Achar, and M. S. Nakhla, "z-domain orthonormal basis functions for physical system identifications," *IEEE Trans. Adv. Packag.*, vol. 33, no. 1, pp. 293–307, Feb. 2010.

[8] N. Wong and C. U. Lei, "IIR approximation of FIR filters via discrete-time vector fitting," *IEEE Trans. Signal Process.*, vol. 56, no. 3, pp. 1296–1302, Mar. 2008.

[9] C. U. Lei and N. Wong, "IIR approximation of FIR filters via discrete-time hybrid-domain vector fitting," *IEEE Signal Process. Lett.*, vol. 16, no. 6, pp. 533–537, Jun. 2009.

[10] C. U. Lei and N. Wong, "Efficient linear macromodeling via discrete-time time-domain vector fitting," in *Proc. Int. Conf. VLSI Design*, Jan. 2008, pp. 469–474.

[11] L. Naredo, "z-Transform-based methods for electromagnetic transient simulations," *IEEE Trans. Power Delivery*, vol. 22, no. 3, pp. 1799–1805, Jul. 2007.

[12] A. Ubolli and B. Gustavsen, "Comparison of methods for rational approximation of simulated time-domain responses: ARMA, ZD-VF, and TD-VF," *IEEE Trans. Power Delivery*, vol. 26, no. 1, pp. 279–288, Jan. 2011.

[13] I. Munteanu and D. Ioan, "Parameter extraction for microwave devices based on 4SID techniques," *IEEE Trans. Magn.*, vol. 35, no. 3, pp. 1781–1784, May 1999.

[14] S. Grivet-Talocia, F. G. Canavero, I. S. Stievano, and I. A. Maio, "Circuit extraction via time-domain vector fitting," in *Proc. Int. Symp. Electromagn. Compat.*, Aug. 2004, pp. 1005–1010.

[15] J. Young, D. Svoboda, and W. Burnside, "A comparison of time- and frequency-domain measurement techniques in antenna theory," *IEEE Trans. Antennas Propag.*, vol. 21, no. 4, pp. 581–583, Jul. 1973.

[16] K. Steiglitz and L. E. McBride, "A technique for the identification of linear systems," *IEEE Trans. Autom. Control*, vol. 10, no. 4, pp. 461–464, Jan. 1965.

[17] P. Regalia and M. Mboup, "Undermodeled adaptive filtering: An a priori error bound for the Steiglitz-McBride method," *IEEE Trans. Circuits Syst. II*, vol. 43, no. 2, pp. 105–116, Feb. 1996.

[18] S. Grivet-Talocia and A. Ubolli, "A comparative study of passivity enforcement schemes for linear lumped macromodels," *IEEE Trans. Adv. Packag.*, vol. 31, no. 4, pp. 673–683, Nov. 2008.

[19] J. O. Smith, *Physical Audio Signal Processing*. W3K Publishing, 2010.

[20] L. Lee and J. Chen, "Strictly positive real lemma and absolute stability for discrete-time descriptor systems," *IEEE Trans. Circuits Syst. I*, vol. 50, no. 6, pp. 788–794, Jun. 2003.

[21] K. Zhou, J. Doyle, and K. Glover, *Robust and Optimal Control*. Englewood Cliffs, NJ, USA: Prentice-Hall, 1995.

[22] G. Gu, "All optimal hankel-norm approximations and their l_{inf} error bounds in discrete-time," *Int. J. Control*, vol. 78, no. 6, pp. 408–423, Apr. 2005.

[23] B. Chen, J. Chen, and S. Shern, "An ARMA robust system identification using a generalized l_p norm estimation algorithm," *IEEE Trans. Signal Process.*, vol. 42, no. 5, pp. 1063–1073, May 1994.

[24] T. Pham and R. Defigueiredo, "Maximum likelihood estimation of a class of non-Gaussian densities with application to l_p deconvolution," *IEEE Trans. Acoust., Speech, Signal Process.*, vol. 37, no. 1, pp. 73–82, Jan. 1989.

[25] Q. Chen, H. Choi, and N. Wong, "Robust simulation methodology for surface-roughness loss in interconnect and package modelings," *IEEE Trans. Comput.-Aided Design Integr. Circuits Syst.*, vol. 28, no. 11, pp. 1654–1665, Nov. 2009.

[26] J. O. Smith, *Spectral Audio Signal Processing*. W3K Publishing, 2009.

[27] C. U. Lei and N. Wong, "WISE: Warped impulse structure estimation for time domain linear macromodeling," *IEEE Trans. Compon., Packag., Manuf. Technol.*, vol. 2, no. 1, pp. 131–139, Jan. 2012.

[28] R. Zeng, "Modified rational function modeling for multi-port high-speed differential circuits," in *Proc. Int. Conf. Microw. Millim. Wave Technol.*, Apr. 2008, pp. 459–462.

[29] M. Swaminathan and A. E. Engin, *Power Integrity Modeling and Design for Semiconductors and Systems*. Englewood Cliffs, NJ, USA: Prentice-Hall, 2007.

[30] L. Tommasi, B. Gustavsen, and T. Dhaene, "Robust transfer function identification via an enhanced magnitude vector fitting algorithm," *IET Control Theory Appl.*, vol. 4, no. 7, pp. 1169–1178, Jul. 2010.

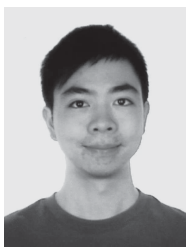

Chi-Un Lei received the B.Eng. (First Class Hons.) and Ph.D. degrees in electrical and electronics engineering from the University of Hong Kong in 2006 and 2011, respectively.

He is currently a Research Scientist with the same university. His research interests include VLSI signal integrity analysis, wireless sensor networks, cyber-physical systems and engineering education.

Dr. Lei was the recipient of the Best Student Paper Award in IAENG IMECS in 2007 and 2010, as well as the Best Paper Award in IAENG IMECS in 2012. He was also a Technical Program Committee Member of the International Symposium on Quality Electronic Design in 2012 and 2013.